ACS OMEGA

Open Access

http://pubs.acs.org/journal/acsodf

Article

PSf Membrane-Impregnated Jute−Copper Nanocomposite as Highly Efficient Dye Removal Material

Harsh Prajapati, Hemen Dave, and Balanagulu Busupalli*

Cite This: *ACS Omega* 2024, 9, 34292−34302

Read Online

ACCESS | Metrics & More | Article Recommendations | Supporting Information

ABSTRACT: Water pollution, driven by the discharge of dyes from industrial processes, poses a significant environmental and health hazard worldwide. Methylene blue, a common dye, constitutes particular concern due to its persistence and toxicity. Conventional wastewater treatment methods often struggle to effectively remove such contaminants. In this study, we introduce a novel approach utilizing a polysulfone-based composite membrane incorporating pretreated jute fibers and copper nanoparticles for the removal of methylene blue from aqueous solutions. The pretreated jute fibers undergo alkali and hydrogen peroxide treatments to enhance their adsorption capabilities, while copper nanoparticles are incorporated into the membrane to bolster its antimicrobial properties. Through comprehensive characterization techniques, including Fourier transform infrared spectroscopy (FTIR), X-ray diffraction (XRD), dynamic light scattering (DLS), and scanning electron microscopy (SEM), we confirm the structural and chemical properties of the composite membranes. Batch adsorption studies reveal the superior performance of the composite membrane compared with individual components. Specifically, at lower methylene blue concentrations (∼20 ppm), the composite membrane demonstrates a remarkable percent removal value of about 97%, while at higher concentrations (∼100 ppm), the percent removal remains substantial at 85%. Additionally, desorption studies elucidate the retention capacity of the adsorbed dye, indicating the feasibility of the composite membrane for practical applications in wastewater treatment. These findings underscore the potential of nanocomposite−fiber membranes as sustainable and cost-effective solutions for mitigating water pollution. By harnessing advancements in nanotechnology and materials science, the presented innovative composite membranes could offer promising avenues for addressing water pollution challenges and promoting environmental sustainability.

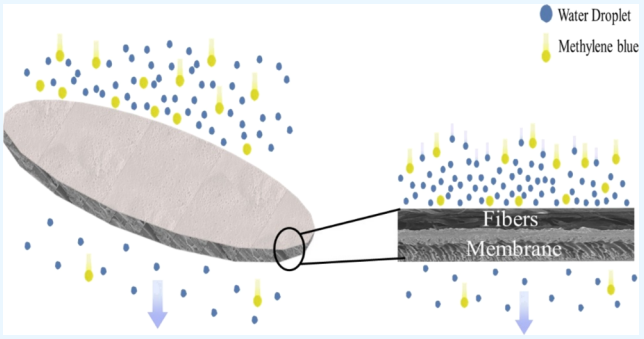

1. INTRODUCTION

Water contamination is a staggering challenge due to different factors including the frequent release of various dyes from several sectors such as textile, papermaking, pharmaceutical, and tannery. Discharging untreated dyes into water streams severely harms the environment. This is because, if left untreated, most dyes would last a very long period in the environment.[1] And their hue makes dyes present in wastewater obvious. Additionally, as sunlight cannot reach plants or algae when water is turbid due to dyes, the ability of the receiving water to reoxygenate will be reduced. The ecosystem's equilibrium is thrown off as a result, which inhibits the oxygenic photosynthesis of aquatic plants or algae.[1−3] Many dyes are also poisonous, mutagenic, and carcinogenic to living things, which is concerning.[4−6]

Most asymmetric polymeric membranes utilized today in membrane separation procedures are made using the phase inversion approach.[7] A homogeneous polymer solution is cast onto a suitable substrate as a thin film in this procedure and is subsequently submerged in a coagulation bath with a suitable nonsolvent. The polymer film solidifies through the interchange of solvents between the nonsolvent outside the cast film and the solvent inside the coagulation bath to create a membrane with a symmetrical or asymmetrical structure. The film undergoes complex phase changes during this solidification process, including liquid−liquid phase separation, solid−liquid phase separation, or both, depending on the polymer's characteristics and the coagulation environment.[7−11] The presence of a thin top layer and a porous sublayer defines the asymmetric membranes. Due to the thin top layer's role as a selective barrier film and the porous sublayer's composition of macrovoids, pores, and micropores, which provides superior mechanical strength, they are frequently employed for gas and liquid separation.

Received: December 13, 2023
Revised: July 9, 2024
Accepted: July 25, 2024
Published: August 2, 2024

Traditional wastewater treatment methods often face challenges in efficiently removing various contaminants, including organic pollutants and pathogenic microorganisms. In recent years, nanotechnology has emerged as a promising avenue for enhancing wastewater treatment processes, offering the potential for improved efficiency, cost-effectiveness, and environmental sustainability.[12−14] Among the diverse array of nanomaterials investigated for wastewater treatment applications, copper nanoparticles have garnered significant attention.[15] Copper nanoparticles possess unique physicochemical properties, including high surface-area-to-volume ratio, excellent catalytic activity, and antimicrobial properties.[16] These attributes make them particularly attractive for addressing the complex challenges associated with wastewater treatment.

In wastewater treatment, copper nanoparticles can be utilized in various ways, including as catalysts for advanced oxidation processes (AOPs), adsorbents for pollutant removal, and antimicrobial agents for disinfection.[17,18] Their ability to efficiently degrade organic pollutants, such as dyes, pharmaceuticals, and industrial chemicals, holds promise for enhancing the efficiency of wastewater treatment systems. Additionally, the antimicrobial properties of copper nanoparticles make them effective in combating microbial contaminants, thereby reducing the risk of waterborne diseases.[19]

Furthermore, the integration of copper nanoparticles into existing wastewater treatment technologies, such as membrane filtration, adsorption processes, and disinfection units, presents opportunities for enhancing treatment efficiency and reducing operational costs.[20] However, despite their potential benefits, the deployment of copper nanoparticles in wastewater treatment requires careful consideration of their environmental impact, potential toxicity, and long-term stability.

Many researchers picked natural jute fiber as an adsorbent material because of its inexpensive cost, which takes care of the financial aspect with reference to its large-scale use. It is also renowned for being environmentally friendly and durable, making it suitable for this use. Due to its high lignin percentage and hemicellulose ratios, jute fiber is also well-recognized for being stiff, having a rough texture on its surface, and having a high crystalline proportion.[21] Low-concentration alkali impregnation of the jute fibers was utilized as a pretreatment to reduce the crystalline percentage about the amorphous component to get around this disadvantage. This thus increases the potential for chemical reactions between the jute strands and the dye.[22−25]

In recent years, nanocomposite materials, including polymeric nanocomposites, have emerged as promising candidates for wastewater treatment due to their exceptional adsorption, catalytic, and antimicrobial properties.[26,27] These materials, composed of a combination of nanoscale particles and a polymeric matrix, offer enhanced performance and efficiency compared with traditional treatment methods. Nanocomposites exhibit high surface-area-to-volume ratios and tenable surface properties, making them ideal for the adsorption and degradation of various pollutants present in wastewater.[13,28]

Moreover, polymeric nanocomposites can serve as excellent catalysts for the degradation of organic pollutants through processes, such as photocatalysis and advanced oxidation. Semiconductor nanoparticles like copper, TiO_2, and zinc oxide (ZnO) are commonly used in polymeric nanocomposites, harnessing solar energy to initiate the degradation of organic compounds into harmless byproducts.[20,29] Furthermore, the incorporation of noble metal nanoparticles such as silver (Ag) or palladium (Pd) into polymeric nanocomposite matrices enhances catalytic activity and provides antimicrobial properties, making them effective in disinfection and removal of pathogens from wastewater.

The development of polymeric nanocomposite materials for wastewater treatment arises from the urgent need for sustainable and cost-effective solutions to combat water pollution challenges. By leveraging advancements in nanotechnology and materials science, researchers strive to engineer polymeric nanocomposites with enhanced performance, stability, and scalability tailored to large-scale applications in wastewater treatment plants. Furthermore, the integration of polymeric nanocomposites into existing treatment processes holds promise for the creation of modular and adaptable systems designed to meet specific water quality requirements.

In this study, our focus centers on embedding pretreated natural jute fibers and copper nanoparticles into a polysulfone polymeric membrane, aiming to create a composite material targeted at removing methylene blue dye from wastewater. Through meticulous batch absorption studies, we assessed the absorption capacity of the composite material across varying initial concentrations of methylene blue dye. This investigation delves into the comparative performance of the different composites prepared, shedding light on their usefulness in dye removal. Through our research efforts, we aim to contribute to the development of efficient and environmentally friendly wastewater treatment methods, addressing the growing concerns surrounding water pollution and resource conservation.

2. MATERIALS AND METHODS

2.1. Materials. Hydrogen peroxide 30% (extra pure), hydrochloric acid (extra pure), methylene blue ($C_{16}H_{18}ClN_3S$) (MB), copper sulfate pentahydrate ($CuSO_4 \cdot 5H_2O$), L-ascorbic acid ($C_6H_8O_6$), polyvinylpyrrolidone (PVP-K30) (typically has a weight-averaged M_w of approximately 40,000 Da (Da) and a polydispersity index (PDI) of around 2.0), sodium hydroxide (NaOH) pellets, sodium azide, poly ethylene glycol (PEG) (Mw of about 400 Da and a PDI between 1.1 and 1.2), polysulfone (PSf), and *N*-methyl pyrrolidone (NMP). Polysulfone (PSf) generally exhibits a PDI between 2.0 and 3.0, suggesting a broad molecular weight distribution, which is typical for many industrial polymers. The molecular weight of PSf is 26,000 g/mol. The water used throughout this work was reagent-grade water produced by deionized water. All of the above-listed polymers and chemical products were purchased from the Hardi-Chem Enterprise, Ahmedabad, India. All of the analytical reagent-grade chemicals were used as received without further purification. Raw jute fibers are purchased from local hardware stores.

2.2. Methods. *2.2.1. Process for Obtaining Treated Jute Fibers.* Jute was washed and oven-dried after being cleaned of all impurities. In the next step, jute was soaked in 20% NaOH solution (5 M NaOH solution) (material:liquor = 1:10) for 48 h. Following this step, the jute was washed with distilled water until pH was neutralized and then it was oven-dried.[30] The purpose of the pretreatment is to remove hemicellulose and lignin from jute. Further to oxidize the NaOH-treated jute, it was immersed in 30% hydrogen peroxide solution (material:liquor = 1:10) for 72 h in basic condition. After this, the material was filtered and washed thoroughly with distilled

https://doi.org/10.1021/acsomega.3c09966
ACS Omega 2024, 9, 34292−34302

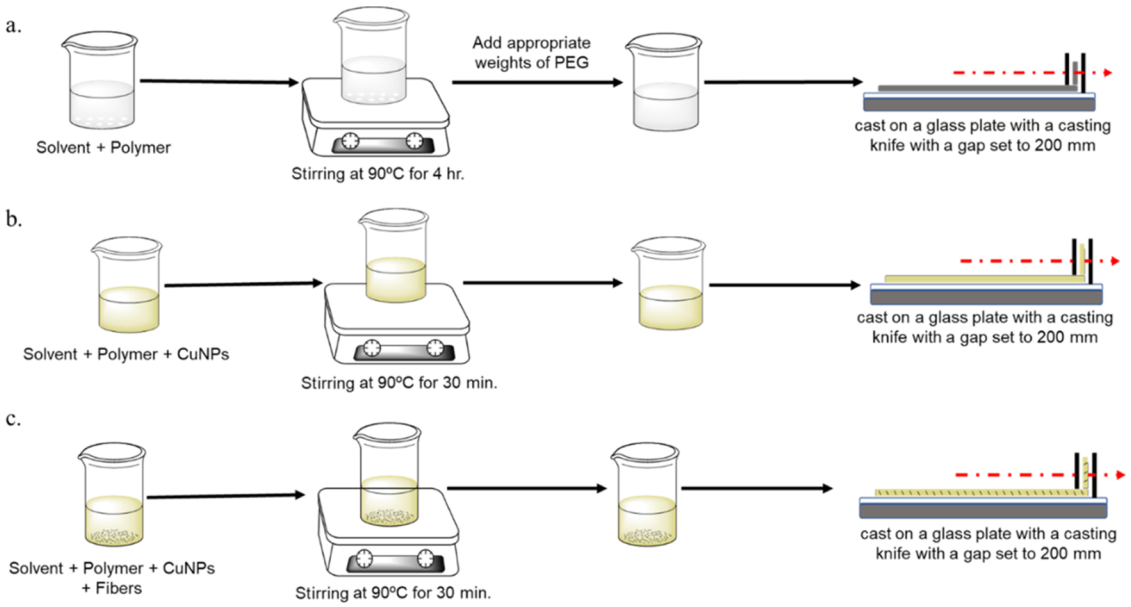

Figure 1. Preparation of different membrane composites: (a) PSf membrane, (b) PSf + NP (composite-1), and (c) PSf + NP + fibers (final composite material-2) (Supporting Figure S1a. Jute fibers, S1b. Phase inversion process and stored in deionized water or azide solution).

Table 1. Details of Prepared Composite Materials (the Ratios (Percentage Ratio) Are Given in Parentheses)

prepared materials	NMP	PSf	CuNPs	jute fibers	PEG	additional modification	weight of the material
PSf	8.0 g (80%)	1.5 g (15%)	–	–	0.5 g (5%)	PSf	0.0851 g
composite-1	7.9 g (79%)	1.5 g (15%)	0.1 g (1%)		0.5 g (5%)	PSf + CuNPs	0.0905 g
composite-2	7.8 g (78%)	1.5 g (15%)	0.1 g (1%)	0.1 g (1%)	0.5 g (5%)	PSf + CuNPs + Jute	0.0947 g
multilayer assembly						composite (PSf + 1 + 2)	0.2504 g
multilayer assembly + backup layered						composite (PSf + 1 + 2) + 1 g jute fibers	0.2504 g (±0.05) + 1 g jute

water. The goal of this process is to convert the primary hydroxyl groups of cellulose found in jute to carboxyl groups, resulting in a weak cationic ion-exchanger.[31] After that, the material was oven-dried, ground, and used as an adsorbent.

2.2.2. Process for Preparing Copper Nanoparticles. 1 g of $CuSO_4$. $5H_2O$ was dissolved in 100 mL of deionized water using magnetic stirring until the solution developed a translucent light blue hue, and this solution was designated as solution A. Solution B was made by dissolving 2.64 g of PVP in 100 mL of deionized water while stirring continuously and then adding 4.5 g of L-ascorbic acid while stirring continuously until the solution became clear. When B reached 85 °C, A was then injected dropwise into B using a constant pressure dropping funnel at a rate of 5 mL/min. The pH of the mixture was adjusted by adding aqueous NaOH to a range of 10−12. The solution underwent a 4 h reaction at 85 °C while being magnetically stirred constantly. The solution progressively changed color over the course of 4 h, going from pale blue to orange and then to reddish-brown (Figure S3). The final liquid sample of the reaction was centrifuged, and the precipitate was collected. To eliminate the excess PVP, unreacted copper ions, and other contaminants, the precipitate was centrifuged with deionized water and ethanol.[32−37]

2.2.3. Process for PSf Membrane Preparation. Polysulfone (PSf) membranes were prepared via the method as follows: (i) PSf (1.5 g) was completely dissolved in NMP solvent (8.0 g) at 90 °C, and then appropriate weights of PEG (0.5 g) were added to the PSf solutions to obtain a porous membrane; (ii) at room temperature, the debubbled polymer solution was cast onto a glass plate with a casting knife with a gap set to 200 μm. The cast liquid film was left for evaporation in air for 20 s before its immersion in a water coagulation bath at 18 °C. A white solid film was stripped out of the glass plate a little moment after the immersion (Figure 1). The coagulated membranes were abundantly washed with water and stored in deionized water or sodium azide solution (Figure S1). The obtained membranes exhibited a glossy surface on the water-bath side, which is the side of the dense layer, and a dull surface on the glass support side. Details of the membrane composites with their specific materials that are used for loading are shown in Table 1.[38−42]

2.2.4. Process for Preparation of Composites-1 and -2. For the preparation of composite-1, first, PSf solution containing CuNPs was prepared. 0.1 g (1%) of CuNPs was taken in a mortar and ground thoroughly with a pestle to get a homogeneous nanoparticle (fine powder) before adding it to the PSf + NMP + PEG mixture; nanoparticles were washed using 2−4 mL of ethanol. The temperature was maintained at 80 °C to avoid the formation and accumulation of small lumps. A slightly yellowish solid film was stripped out of the glass plate a little after the immersion. The coagulated membranes were abundantly washed with water and stored in deionized water or sodium azide solution. For the preparation of the final composite-2, 0.1 g (1%) of finely ground pretreated jute was

https://doi.org/10.1021/acsomega.3c09966
ACS Omega 2024, 9, 34292−34302

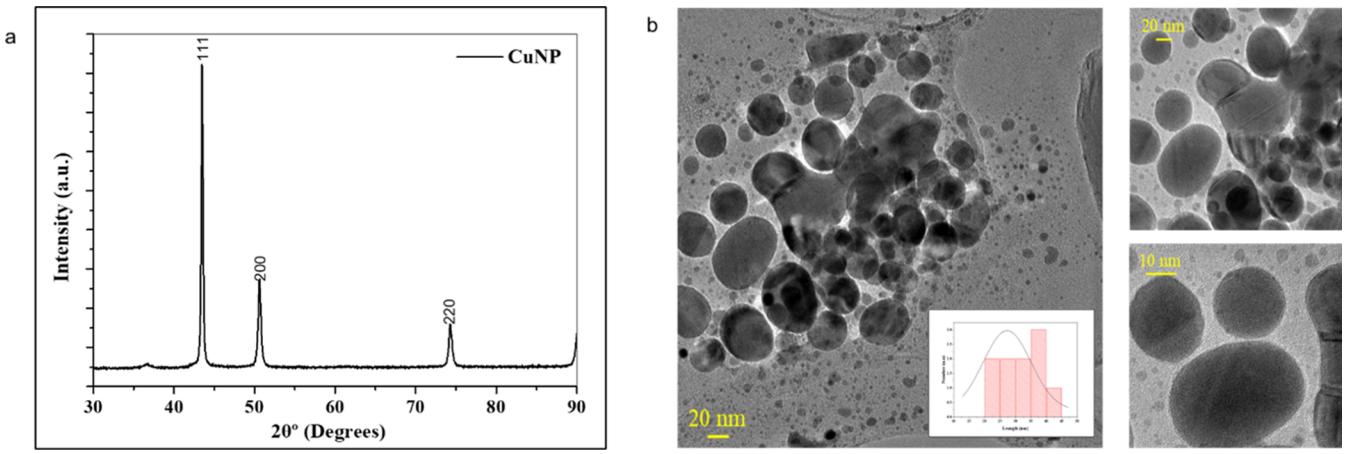

Figure 2. (a) XRD of copper nanoparticles and (b) TEM of copper nanoparticles.

added in addition to the already added CuNPs. During the addition of finely ground jute, the jute powder has to be passed through the finest available sieves. After that, the membrane containing the CuNPs along with the jute fibers in it was cast in a similar way as that described in the previous method.

2.3. Instrumental Methods. All samples were studied by ultraviolet−visible (UV−vis) absorption spectroscopy, employing a LABINDIA Analytical 3000^{+} instrument. For the absorption study of the MB, we have taken initial MB dye samples and the samples after passing the MB aqueous solutions through different composite materials and collected the filtrates and then taken in UV−vis quartz cuvettes, and the spectra were obtained for these samples at a fixed wavelength of 664 nm. The presence of functional groups in different samples employed in this study was checked by Fourier transform infrared spectroscopy (FTIR) spectra using a PerkinElmer Spectrum Two. FTIR analysis of all samples has been carried out in solid from without crushing or cutting. The particle size and size distribution of NPs were determined by dynamic light scattering (DLS) using the Malvern Zetasizer Nano ZS90 with a 4 mW power He−Ne red laser source having a wavelength of about 633 nm. DLS measurements were performed by dispersing 10 mg of CuNP powder in 20 mL of deionized water. The solution was stirred in a vortex mixer for 5−10 min to break up any aggregates, and then 1−2 mL was transferred to the zeta-disposable cell. The structure of the synthesized nanoparticles and membrane composites was analyzed with X-ray diffraction (XRD) (PANalytical X'Pert Pro) with Cu Kα (0.15418 nm) as the source to study the crystallographic phases. XRD patterns were recorded from 2θ degrees 10 to 80° with a scanning step of 0.02°. Using the Scherrer equation, we find the crystallite size

$$D = \frac{K\lambda}{\beta \cos\theta}$$

where D is the crystallite size, K is the Scherrer constant (usually 0.9), β is the full width at half-maximum (fwhm) (or fwhm) (in radians) (also called PWHM or pwhm), and λ is the 0.15418 nm. $\cos\theta$ was converted to cos radians for calculation purpose.[43,44]

The morphological study of the membranes and nanoparticles was performed by scanning electron microscopy (Zeiss ultra-55) for microstructural characterization and field emission scanning electron microscopy for membrane cross section JSM7600F (JEOL). For imaging the cross section of the membranes, the membranes were cut and sputter-coated with gold for 1−2 min. The cross-sectional images of the final composite (composite-2) were obtained at different magnifications. Transmission electron microscopy (TEM, JEOL, JEM 2100) analysis of copper nanoparticles involves using an electron beam to pass through a thin sample, providing high-resolution images of the nanoparticles. Samples for TEM measurements were suspended in ethanol and ultrasonically dispersed. Drops of the suspensions were placed on a copper grid coated with carbon. This technique allows for a detailed observation of the size, shape, and distribution of the copper nanoparticles. These images were analyzed by ImageJ software.

The formula used for the calculation of % removal is

$$\%\ \text{removal} = \frac{I^{\circ} - I}{I^{\circ}} \times 100$$

where I° is the initial concentration, and I is the final concentration.

3. RESULTS AND DISCUSSION

Fourier transform infrared spectroscopy (FTIR) shown in Figure S2 presents a comprehensive examination of the untreated and treated jute fibers, elucidating their chemical composition and structural alterations in detail. Within the spectral region spanning from 3330 to 1630 cm^{-1}, the untreated jute manifests subtle absorption patterns, indicating OH− bending and OH− stretching frequencies, whose intensity is relatively low due to their interaction with lignin, waxes, and hemicelluloses. Notably, the absorption band observed at 2895 cm^{-1} corresponds to CH_2 groups, whose intensity undergoes enhancement following treatments, suggesting an augmentation in pure cellulose content, attributable to the reinforced intensity of CH_2^- groups within cellulose molecules' β-glucoside rings. Furthermore, the presence of lignin is discerned by the absorption band at 1725 cm^{-1}, linked to the aromatic ring vibration, while acetyl or ester groups in hemicelluloses are identified by peaks within the 1700−1740 cm^{-1} range.[45,46] The absence of these distinctive peaks in bleached fibers denotes the complete elimination of lignin and hemicelluloses during processing, leaving behind a cellulose-rich material. Chemical treatments, as delineated by FTIR analysis, result in a reduction in the quantity of binding components within the fibers, reflecting alterations in their chemical composition.[47]

https://doi.org/10.1021/acsomega.3c09966
ACS Omega 2024, 9, 34292−34302

Moreover, the interaction between copper nanoparticles (CuNPs) and various functional groups[34] is elucidated by intense bands at 1637 cm^{-1} (corresponding to the carbonyl stretching of amide) and 3305 cm^{-1} (attributed to NH_2 and −OH groups) (Figure S4a). The presence of these bands suggests a strong affinity between CuNPs and functional groups on the jute fiber surface. Additionally, the FTIR analysis provides insights into the interaction among materials within composite-2 in Figure S6, highlighting specific bands associated with etheric stretching, symmetric and asymmetric stretchings of sulfone groups, and various other molecular vibrations, thus offering a meticulous characterization of the composite's chemical structure and composition while ensuring the inclusion of all relevant group and intensity details.[19,48] The phase crystallinity and structural aspects of the synthesized copper nanoparticles were analyzed by powder X-ray diffraction. Figure 2a represents the diffraction pattern of Cu nanoparticles in which the peaks at 2θ values of 43.49, 50.61, and 74.31° correspond to (111), (200), and (220) planes, respectively, confirming the cubic lattice of copper. All of the diffraction peaks are in good agreement with the standard pattern for the pure face-centered cubic phase of copper nanoparticles (JCPDS No. 040836).[49] CuNPs prepared were highly crystalline,[50,51] and the average particle size was around 50 nm; that is why the peaks in powder XRD corresponding to the copper nanoparticles are sharp. A minute impurity peak of CuO or Cu_2O was observed. Besides the metallic Cu peaks, one very small diffraction peak appeared at 36.54° corresponding to the (110) plane of cuprite, which indicates the formation of cubic copper(I) oxide nanocrystals.[52,53] Using the Scherrer equation, we calculate that the crystallite size of the copper nanoparticles for plane (111) is 80.87 nm, for plane (200), it is 39.98 nm, and for plane (220), it is 19.24 nm. The average crystallite size for CuNPs is 46.69 nm. This is in agreement with the particle size obtained from the DLS measurement. The instrument broadening pwhm is 0.05°. The pwhm for the Cu sample for the plane (111) in 2θ is 0.26767°, and after conversion to radians, it is 0.00467, for the plane (200) 2θ, it is 0.46525°, and after conversion to radians, it is 0.0081, and for the plane (220) 2θ, it is 0.65853° and after conversion to radians, it is 0.0114. XRD peaks observed (Figure 2) for cuprite were matched well with the standard powder diffraction card of bcc cuprite (JCPDS No. 05−667).[54] The relatively high intense peaks (more than 20 times more intense compared to the insignificant impurity peak of copper oxide) corresponding to CuNPS in the spectra indicate the highly crystalline nature of the sample, and the significant broadening of peaks is attributed to the nanocrystalline nature of the Cu nanoparticles.[32,49,55] TEM images of CuNPs in solution showed the particles to be mainly spherical, nanocrystalline, and monodisperse (Figure 2b). Although some nanoparticle agglomeration was observed, with evidence of clusters ∼40 nm in diameter, overall, size analysis is shown. Narrow size control was achieved by using the antioxidant, L-ascorbic acid, which was effective in reducing Cu^{2+} to Cu(0) and capping the CuNPs, such that the resulting particles were small and stable.[50,55]

The XRD spectra of untreated and treated jute fibers are shown in Figures S7−S10. The ratio of cellulose Iα and Iβ from various origins has been determined by many methods. After deconvolution, we found that the XRD spectra showed that the cellulose increase to peak at around 2θ = 16.03° is the composite peak of (1−10 and 110) planes, 22.30° for the plane (200), and 34.5° for the plane (004) in raw fiber, which are respectively, 15.73° (1−10) and 22.25° (200) in alkali-treated fiber and 21.20° after bleaching treatment. A small peak at 12° for the (1−10) plane of cellulose II and another peak at 21.20° are a combination of (110) and (020).[56] The peak at 34.5° for the plane (004) indicates that both celluloses I and II are present but usually a very weak peak for cellulose II[56,57] (ref codes: 00−003−0226, 00−003−0203) or the presence of both. After the bleaching treatment, the surface of jute fiber becomes highly amorphous because of the opening of microfibrils inside the jute fibers. During this process, a loss of weight of jute fibers occurs due to the removal of the cementing materials including lignin, waxes, and hemicelluloses. This treatment increases the amorphous regions.[58−60] All other details of XRD data are mentioned in Table 2 and Figure 3a. Figure 3b shows the final composite (composite-2) XRD patterns that indicate that the material is mostly amorphous. PSf membrane has a broad diffraction peak with a maximum of 18.5°, which matches with the previously reported literature.[61]

Table 2. Jute Fibers' XRD Peak Details with FWHM (PWHM) Values Along with the Calculated Crystallite Sizes

samples	2θ	fwhm (PWHM)	crystallite size
raw fibers	16.03°	5.011°	–
	22.32°	2.86°	2.96 nm
alkali-treated fibers	15.73°	3.72°	2.24 nm
	22.36°	2.68°	3.16 nm
after bleaching treatment	12°	2.26°	3.69 nm
	21.20°	3.95°	–

Dynamic light scattering (DLS) measurements give information about the surface charge and size of nanoparticles. The average particle size distribution of the synthesized CuNPs in the present work is around 50−60 nm; the values are consistent with the followed literature[62,63] (Figure S4b). Scanning electron microscopy (SEM) micrographs of the fibers, both in their natural state and after chemical processing, were obtained. By comparison of the images taken before and after the bleaching operation, the SEM micrographs demonstrate the variations in the fiber surfaces. When compared with the surface of the raw fibers, the treated fiber surfaces are smoother and have less number of solid aggregates. Although alkali treatment is more effective for impurity removal, the impurities could not be totally removed just by alkali treatment shown in Figure 4a. Figure 4b shows that the bleached jute fiber had a clearer and smoother surface than the untreated jute. So, it was clear that the residual impurities on the alkali-treated jute fiber could be further removed by hydrogen peroxide bleaching. As shown in Figure 4b, there are many gaps and microvoids on the treated jute fiber surface. These microvoids and gaps provide access to the other materials, which is beneficial for improving the interfacial compatibility and mechanical properties of composites.[64,65] The morphological characterization of CuNPs (Figure 4c) was carried out using SEM−energy-dispersive system (SEM−EDS) analyses (Figure S11). SEM analysis revealed the presence of spherical particles with some agglomeration resulting during the sample preparation.[55] SEM analysis of the final composite (composite-2) shown in Figure 4d,d.1,d.2 clearly reveals that the nanoparticles and fibers are properly embedded into the membrane.[66]

https://doi.org/10.1021/acsomega.3c09966
ACS Omega 2024, 9, 34292−34302

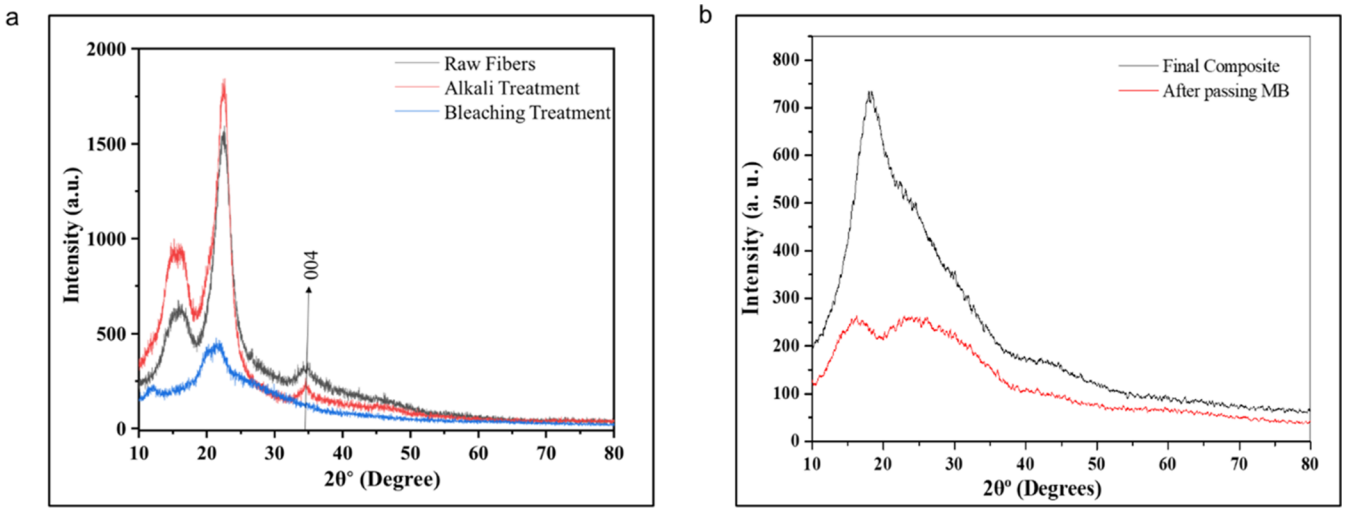

Figure 3. (a) Jute fiber and (b) before and after passing MB from the final composite (composite-2).

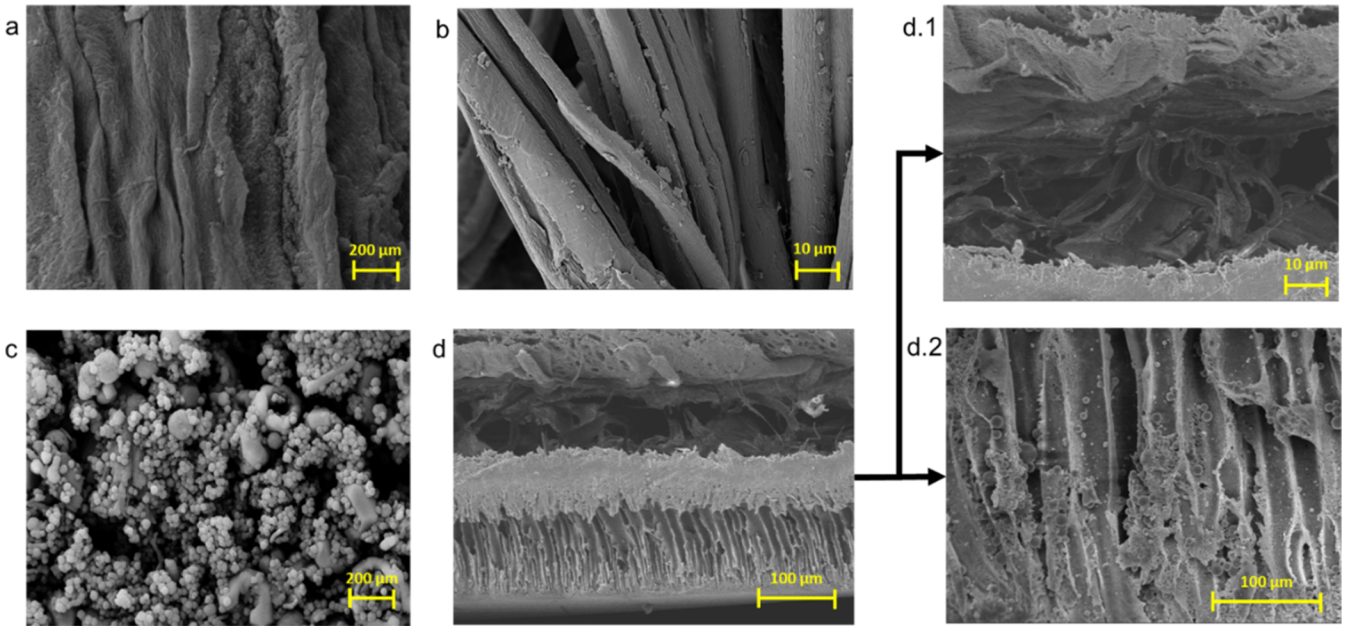

Figure 4. (a) SEM of jute fibers before pretreatment. (b) SEM of jute fibers after pretreatment. (c) SEM of copper nanoparticles. (d, d.1, d.2) The cross section of the final composite (composite-2).

3.1. Composite Performance in the Removal of Methylene Blue (MB) Dye % Removal. The experimental results for removing MB from the aqueous solution using membrane separation at various concentrations (20, 40, 60, 80, and 100 mg/L) of MB (Figure 5a) and with a comparative study of different composite materials are provided in Figure 5b.[67,68] Percent adsorption decreased with an increase in the initial MB concentration in the case of PSf, composite-1, and composite-2. In the multilayer setup (PSf + 1 + 2 as mentioned in Table 1), around 90% removal in lower concentration (20 ppm) was observed, whereas in the higher concentration (100 ppm), removal of around 54% was observed as compared to the separate dye removal materials, viz., composite-PSf, 1, 2. The multilayer setup made out of both the composites-1 and 2 along with the backup layer of jute fibers exhibited the removal of MB ∼40% higher (around 97% in lower concentration and 85% in higher concentration) than any other setups.

The adsorption of methylene blue onto jute fiber surfaces involves a complex interplay of electrostatic interactions, hydrogen bonding, van der Waals forces, and chemical bonding. Being positively charged, methylene blue is initially attracted to the negatively charged jute fiber surface due to electrostatic attraction, facilitated by functional groups like carboxylate and hydroxyl ions.[69] Hydrogen bonding stabilizes this interaction, while weak van der Waals forces contribute to adsorption. The pH of the dye bath influences the adsorption process, with higher pH values favoring dye uptake due to increased negative charge on the fibers.[70] Temperature affects the kinetics of adsorption, with higher temperatures promoting faster dye uptake. Understanding these chemical mechanisms that are shown in Scheme 1 is essential for optimizing adsorption conditions to achieve high efficiency for the removal of methylene blue dye using jute fiber-impregnated membrane. The COOH groups of cellulose become deprotonated and create COO^- groups on the jute surface.

https://doi.org/10.1021/acsomega.3c09966
ACS Omega 2024, 9, 34292−34302

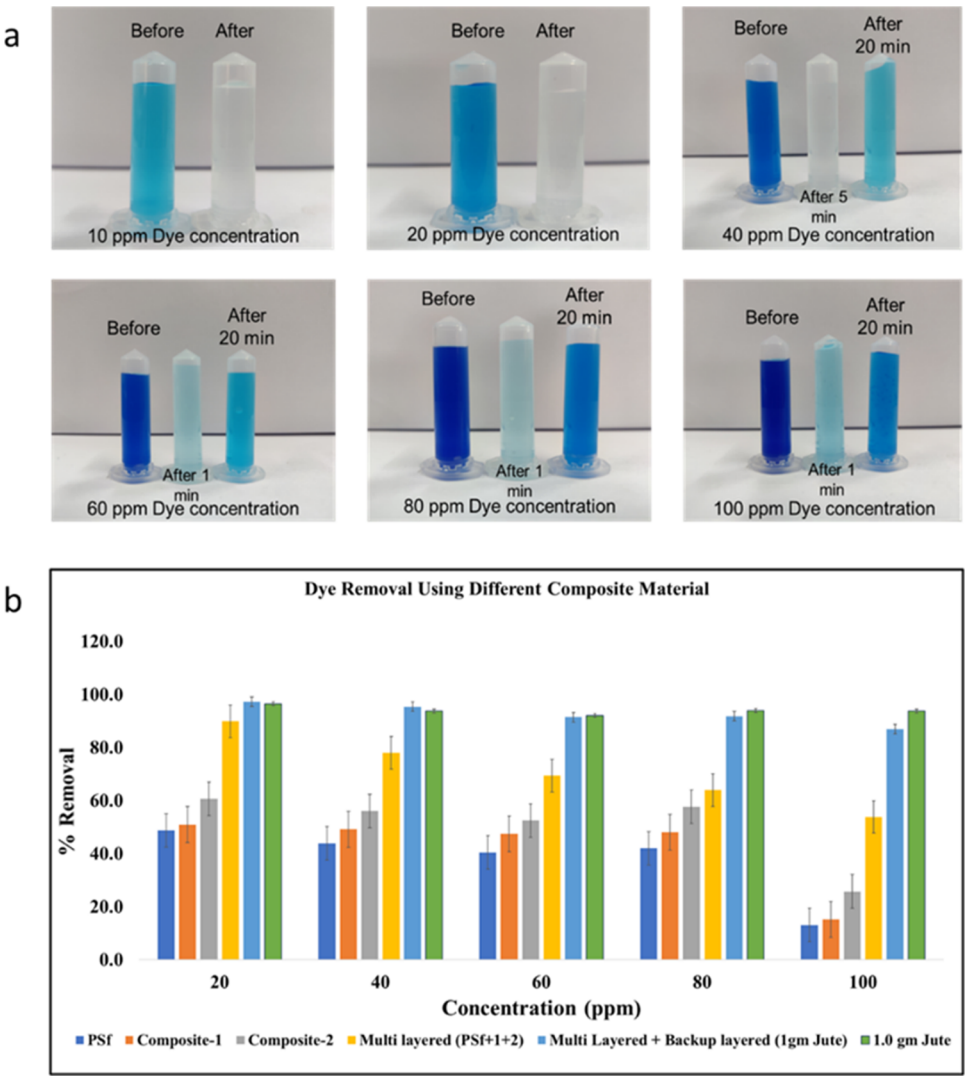

Figure 5. (a) Removal of MB dye using final composite-2 and (b) comparison of different composites to check % removal of MB dye.

Thus, the electrostatic attraction between the above-mentioned negative charge on the surface of the jute fibers and the positive ion of the dye can react (Scheme 1). MB is a planar molecule, and it can easily be adsorbed on cellulose-based adsorbents. And it can also be adsorbed by van der Waals force and hydrogen-bonding interactions.

3.2. Study of Adsorption and Desorption of MB Dye Using Only Jute Fibers. Adsorption capacity of the jute fibers as the sole adsorbent was tested (Figure 6a,b), and it was found that the maximum adsorption at lower concentration (20 ppm) was around 98% and an adsorption efficiency of 95% in higher concentration (100 ppm). This adsorption study was carried out on a shaker after adding 1 gm of jute fiber in the dye-contaminated water. % Removal is shown in Figure 6c. Though the adsorption capacity of the sole adsorbent jute fibers is high, desorption studies on the same jute fibers to obtain data on the retention capacity of the adsorbed MB dye at different MB dye concentrations revealed that employing only jute fibers for the adsorption of dyes is not a viable option as the retention of the dyes in the jute fibers is meager (Figure 6d). These time-dependent desorption experiments revealed that the MB dye could not be retained in only jute fibers as much as in line with that of composite-3, indicating that the multilayered composite consisting of composite-3 and the backup jute layers (Figure S12 displaying the complete filtration setup) could give excellent results in MB dye removal rather than just with only jute, as most of the desorption of MB dye was observed just after 10−15 min of adsorption in the only jute sample.

The observed increase in desorption (%) from 10 to 15 min for the 20 ppm MB solution likely indicates a saturation point where dye molecules on the jute surface desorb more rapidly due to weaker binding forces at lower concentrations. For the 60 ppm MB solution, a significant increase in desorption (%) from 25 to 30 min may result from stronger initial binding interactions that weaken over time, leading to a higher desorption rate. Error bars representing the standard error of the mean are added to Figure 6c,d to enhance the clarity and scientific rigor of the manuscript. Various desorbing agents, such as neutral deionized water, HCl, NaOH, and CH_3COOH, are available, but in this study, dye-loaded jute fiber was washed with deionized water to remove any unabsorbed dye.

4. CONCLUSIONS

PSf membrane modification using nanoparticles and jute fibers to obtain a novel PSf + NPs + jute composite for MB dye

https://doi.org/10.1021/acsomega.3c09966
ACS Omega 2024, 9, 34292−34302

Scheme 1. Representation of the Chemistry Involved in the Adsorption of the MB Dye onto the Cellulose in the Composite Containing the Jute Fibers

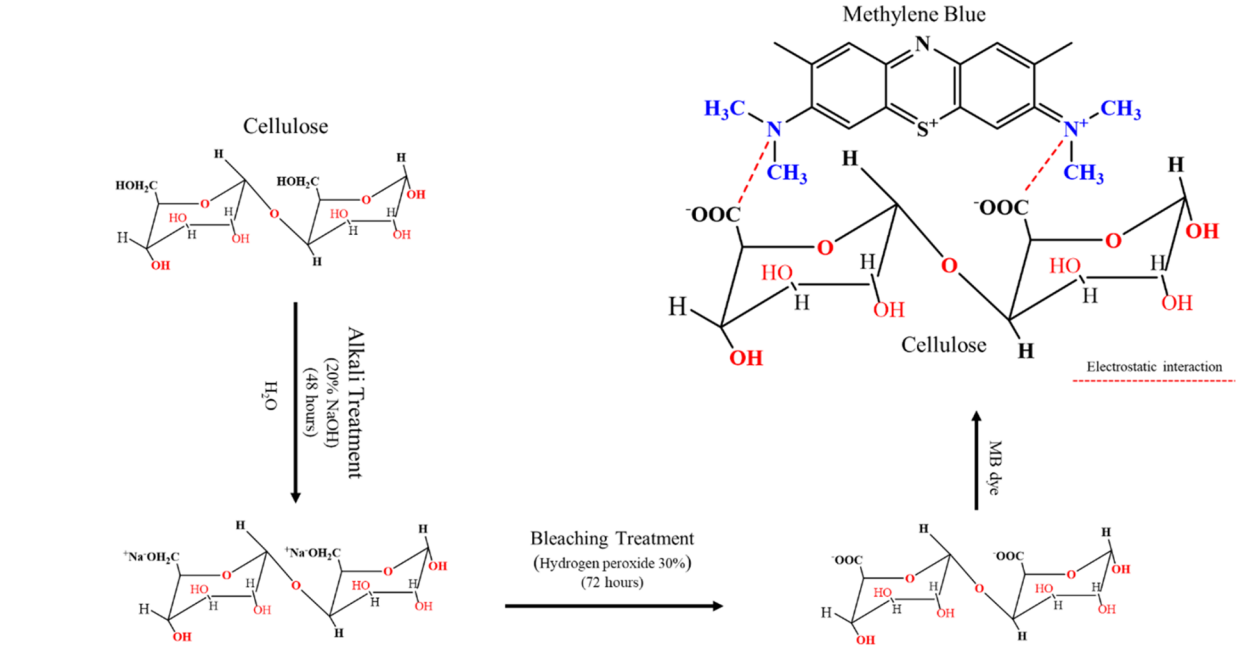

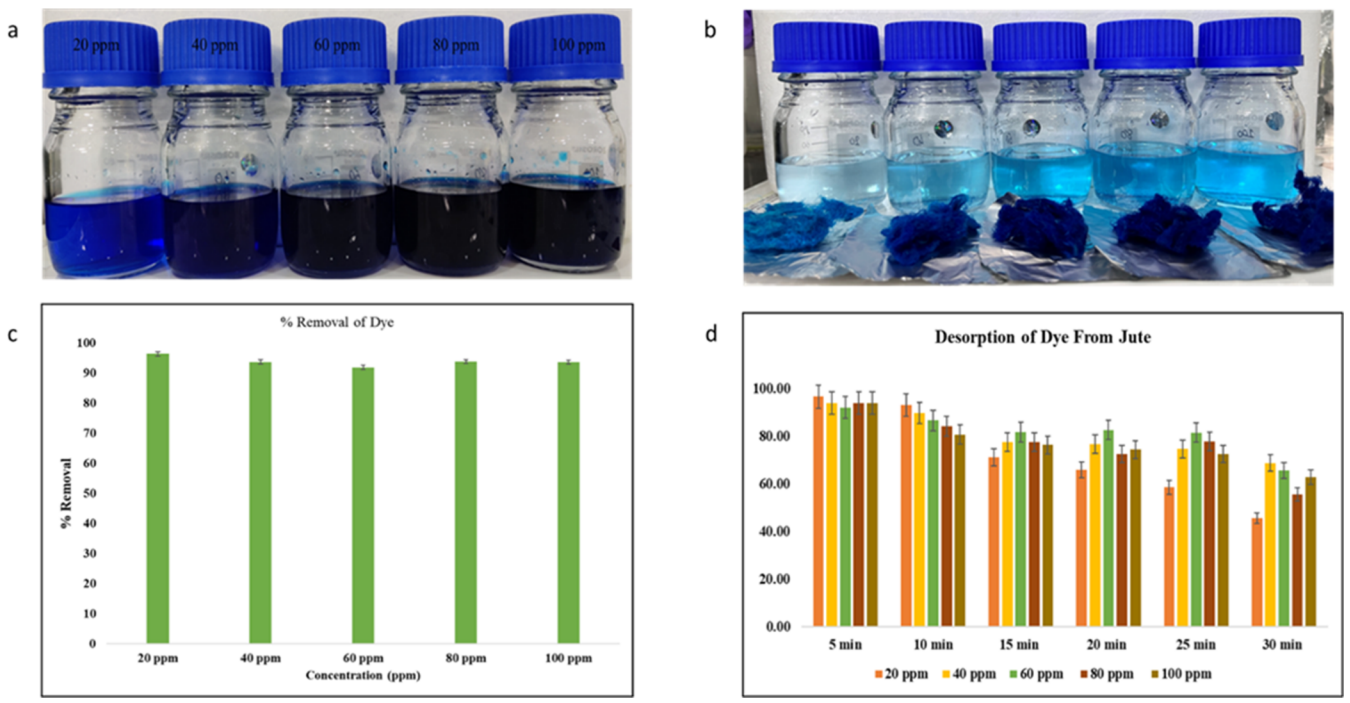

Figure 6. Photographic images representing the experimental observations of "only jute" as test material: (a) initial dye concentration, (b) after adsorption of the dye onto the only jute material, (c) % removal of the dye, and (d) desorption of the dye from the "only jute" surface.

removal was performed in this study. The composite membrane exhibited better physical and chemical properties than the ordinary one. Natural jute fiber has been observed to be a good adsorbent material. Here, we show jute fibers embedded in the composite polymer membrane containing copper nanoparticles as the best adsorbent in the case of cationic dye removal processes. We found the desorption of MB dye just after 10−15 min of adsorption from the adsorbent sample employing only jute fibers, ruling out the possibility of utilization of only jute in such water purification systems. Rather, through our thorough experimentation, it was revealed that the composite along with jute layers resulting in a final multilayered composite jute system is best for removing the cationic MB dye even at low concentrations. As mentioned in the literature for the better adsorption of anionic and cationic dyes, the materials require great modifications but the required modifications are usually very costly. To mitigate the pricey nature of the required modifications in the adsorbent materials to remove ionic dyes such as MB dye and to validate very cheap materials such as jute fibers in such water purification

https://doi.org/10.1021/acsomega.3c09966
ACS Omega 2024, 9, 34292−34302

processes, we, in the present study, demonstrated that polymeric composite materials with jute layers could become better adsorbent materials for the dye removal. In this work, we prepared three different composites in total, as mentioned in Table 1. We observed that with the increase in MB concentration, adsorption is decreased in the PSf and composites-1 and -2. In the multilayer setup too, adsorption is decreased when we increase the concentration. However, with the backup layered material (consisting of the multilayer + jute), we get 40% higher adsorption than the other setups. With further chemical modification of the treated fibers, we hope to increase the membrane strength further and enhance its selectivity in adsorption. Based on the present discussion, there is a huge opportunity to use nanocomposite−fiber membranes in industrial as well as domestic applications.

■ ASSOCIATED CONTENT

Supporting Information

The Supporting Information is available free of charge at https://pubs.acs.org/doi/10.1021/acsomega.3c09966.

Additional images for the jute fibers; storage of the casted membrane in deionized water or azide solution; schematic representation of the preparation of copper nanoparticles; DLS data of copper nanoparticles; additional FTIR, XRD spectra, SEM−EDX images of membrane; discussion on the XRD data of jute fibers indicating cellulose I and II; and filtration setup (PDF)

■ AUTHOR INFORMATION

Corresponding Author

Balanagulu Busupalli − *Department of Chemistry, Pandit Deendayal Energy University (PDEU), Gandhinagar, Gujarat 382426, India;* orcid.org/0000-0001-5530-0463; Email: baalanaagulu@gmail.com, busupalli.balanagulu@sot.pdpu.ac.in

Authors

Harsh Prajapati − *Department of Chemistry, Pandit Deendayal Energy University (PDEU), Gandhinagar, Gujarat 382426, India*

Hemen Dave − *National Forensic Sciences University, Gandhinagar, Gujarat 382007, India*

Complete contact information is available at: https://pubs.acs.org/10.1021/acsomega.3c09966

Author Contributions

H.P. and B.B. wrote the manuscript and prepared all figures. H.D. also contributed to writing. H.P. performed all experiments.

Funding

PDEU milestone grant ORSP/R&D/PDPU/2019/BB00/RO048.

Notes

The authors declare no competing financial interest.

■ ACKNOWLEDGMENTS

The authors acknowledge the SHODH scheme of the Gujarat Government ref No. 202101584 for a fellowship for H.P and PDEU for the milestone grant ORSP/R&D/PDPU/2019/BB00/RO048 for B.B. The authors thank SRDC PDEU for SEM.

■ REFERENCES

(1) Carmen, Z.; Daniel, S. Textile Organic Dyes—Characteristics, Polluting Effects and Separation/Elimination Procedures from Industrial Effluents—A Critical Overview. In *Organic Pollutants Ten Years After the Stockholm Convention—Environmental and Analytical Update*; Puzyn, T., Ed.; InTech, 2012.

(2) Zaharia, C.; Suteu, D.; Muresan, A.; Muresan, R.; Popescu, a. Textile wastewater treatment by homogeneous oxidation with hydrogen peroxide. *Environ. Eng. Manage. J.* **2009**, *8* (6), 1359−1369.

(3) Manna, S.; Das, P.; Roy, D. Dye-Containing Wastewater Treatment Using Treated Jute. In *Waste Management and Resource Efficiency*; Ghosh, S. K., Ed.; Springer: Singapore, 2019; pp 1263−1270.

(4) Yahagi, T.; Degawa, M.; Seino, Y.; Matsushima, T.; Nagao, M.; Sugimura, T.; Hashimoto, Y. Mutagenicity of Carcinogenic Azo Dyes and Their Derivatives. *Cancer Lett.* **1975**, *1*, 91−96.

(5) Nair, P. G.; Vijayakumar, S.; Lisluke, T.; Mathew, M. S. P.; Aravindakumar, C. T. Degradation of Dyestuff Pollutant Sudan I Using Advanced Oxidation Process. *J. Water Resour. Prot.* **2014**, *06* (14), 1276−1283.

(6) Nqombolo, A.; Mpupa, A.; Moutloali, R. M.; Nomngongo, P. N. Wastewater Treatment Using Membrane Technology. In *Wastewater and Water Quality*; Yonar, T., Ed.; InTech, 2018.

(7) Mulder, M. *Basic Principles of Membrane Technology*; Springer: Netherlands, Dordrecht, 1996.

(8) Munari, S.; Bottino, A.; Roda, G. C.; Capannelli, G. Preparation of Ultrafiltration Membranes. State of the Art. *Desalination* **1990**, *77*, 85−100.

(9) Reuvers, A. J.; van den Berg, J. W. A.; Smolders, C. A. Formation of Membranes by Means of Immersion Precipitation. *J. Membr. Sci.* **1987**, *34* (1), 45−65.

(10) Ezugbe, E. O.; Rathilal, S. Membrane Technologies in Wastewater Treatment: A Review. *Membranes* **2020**, *10* (5), No. 89.

(11) Pandya, A.; Shah, K.; Prajapati, H.; Vishwakarma, G. S. GQD Embedded Bacterial Cellulose Nanopaper Based Multi-Layered Filtration Membranes Assembly for Industrial Dye and Heavy Metal Removal in Wastewater. *Cellulose* **2021**, *28* (16), 10385−10398.

(12) Lu, H.; Wang, J.; Stoller, M.; Wang, T.; Bao, Y.; Hao, H. An Overview of Nanomaterials for Water and Wastewater Treatment. *Adv. Mater. Sci. Eng.* **2016**, *2016*, No. 4964828.

(13) Hani, U. Comprehensive Review of Polymeric Nanocomposite Membranes Application for Water Treatment. *Alexandria Eng. J.* **2023**, *72*, 307−321.

(14) Kim, A.; Moon, S. J.; Kim, J. H.; Patel, R. Review on Thin-Film Nanocomposite Membranes with Various Quantum Dots for Water Treatments. *J. Ind. Eng. Chem.* **2023**, *118*, 19−32.

(15) Madhusha, C.; Jayasundara, T.; Munaweera, I.; Perera, C.; Wijesinghe, G.; Weerasekera, M.; Sandaruwan, C.; Meiyazhagan, A.; Hernandez, F. C. R.; Ajayan, P. M.; Kottegoda, N. Synthesis and Structural Characterization of Copper Nanoparticles Doped Activated Carbon Derived from Coconut Coir for Drinking Water Purification. *Mater. Today Chem.* **2023**, *27*, No. 101312.

(16) Yegani, R.; Ranjbaran, N.; Akbari, A.; Roghani-Mamaqani, H.; Chapalaghi, M. Graphene Oxide Decorated Copper Nanoparticles Embedded Polysulfone Nanocomposite Membrane: Anti-Bacterial, Organo-Bio Fouling Characteristics and Performance Evaluation in Pharmaceutical Wastewater Treatment Via Mbr. 2024 DOI: 10.2139/ssrn.4758704.

(17) Biju, R. Photocatalytic Degradation of Organic Dyes Using Transition Metal Based Mixed Metal Oxide Nanocomposite under Different Illumination. *Charact. Appl. Nanomater.* **2023**, *6* (2), No. 3573.

(18) Liu, M.; Ye, Y.; Xu, L.; Gao, T.; Zhong, A.; Song, Z. Recent Advances in Nanoscale Zero-Valent Iron (nZVI)-Based Advanced Oxidation Processes (AOPs): Applications, Mechanisms, and Future Prospects. *Nanomaterials* **2023**, *13* (21), No. 2830.

(19) Kheirieh, S.; Asghari, M.; Afsari, M. Application and Modification of Polysulfone Membranes. *Rev. Chem. Eng.* **2018**, *34* (5), 657−693.
(20) Bonthula, S.; Bonthula, S. R.; Pothu, R.; Srivastava, R. K.; Boddula, R.; Radwan, A. B.; Al-Qahtani, N. Recent Advances in Copper-Based Materials for Sustainable Environmental Applications. *Sustainable Chem.* **2023**, *4* (3), 246−271.
(21) Khan, M. A.; Shehrzade, S.; Hassan, M. M. Effect of Alkali and Ultraviolet (UV) Radiation Pretreatment on Physical and Mechanical Properties of 1, 6-hexanediol Diacrylate−Grafted Jute Yarn by UV Radiation. *J. Appl. Polym. Sci.* **2004**, *92* (1), 18−24.
(22) Mwaikambo, L. Y.; Ansell, M. P. Chemical Modification of Hemp, Sisal, Jute, and Kapok Fibers by Alkalization. *J. Appl. Polym. Sci.* **2002**, *84* (12), 2222−2234.
(23) Mohanty, A. K.; Khan, M. A.; Hinrichsen, G. Surface Modification of Jute and Its Influence on Performance of Biodegradable Jute-Fabric/Biopol Composites. *Compos. Sci. Technol.* **2000**, *60* (7), 1115−1124.
(24) Roy, A.; Chakraborty, S.; Kundu, S. P.; Adhikari, B.; Majumder, S. B. Lignocellulosic Jute Fiber as a Bioadsorbent for the Removal of Azo Dye from Its Aqueous Solution: Batch and Column Studies. *J. Appl. Polym. Sci.* **2013**, *129* (1), 15−27.
(25) Hassan, M. S. Removal of Reactive Dyes from Textile Wastewater by Immobilized Chitosan upon Grafted Jute Fibers with Acrylic Acid by Gamma Irradiation. *Radiat. Phys. Chem.* **2015**, *115*, 55−61.
(26) Zhang, F.; Na, H.; Carrier, J.; Chang, C.-Y.; Radu, D.; Lai, C.-Y. Lignin-Based Nanospheres as Environmental Remediation Platforms for Anionic Dye Contaminants. *ACS Omega* **2024**, *9* (10), 12006−12014.
(27) Ciawi, Y.; Khoiruddin, K. Low-Cost Antibacterial Ceramic Water Filters for Decentralized Water Treatment: Advances and Practical Applications. *ACS Omega* **2024**, *9*, 12457−12477.
(28) Divya, S.; Oh, T. H. Polymer Nanocomposite Membrane for Wastewater Treatment: A Critical Review. *Polymers* **2022**, *14* (9), No. 1732.
(29) Khan, N.; Tabasi, Z. A.; Liu, J.; Zhang, B. H.; Zhao, Y. Recent Advances in Functional Materials for Wastewater Treatment: From Materials to Technological Innovations. *J. Sci. Eng.* **2022**, *10* (4), No. 534.
(30) Hassan, M. S.; Zohdy, M. H. Adsorption Kinetics of Toxic Heavy Metal Ions from Aqueous Solutions onto Grafted Jute Fibers with Acrylic Acid by Gamma Irradiation. *J. Nat. Fibers* **2018**, *15* (4), 506−516.
(31) Shukla, S. R.; Pai, R. S. Adsorption of Cu(II), Ni(II) and Zn(II) on Modified Jute Fibres. *Bioresour. Technol.* **2005**, *96* (13), 1430−1438.
(32) Sundar, S.; Venkatachalam, G.; Kwon, S. Biosynthesis of Copper Oxide (CuO) Nanowires and Their Use for the Electrochemical Sensing of Dopamine. *Nanomaterials* **2018**, *8* (10), No. 823.
(33) Mondal, P.; Sinha, A.; Salam, N.; Roy, A. S.; Jana, N. R.; Islam, S. M. Enhanced Catalytic Performance by Copper Nanoparticle−Graphene Based Composite. *RSC Adv.* **2013**, *3* (16), 5615−5623.
(34) Khan, A.; Rashid, A.; Younas, R.; Chong, R. A Chemical Reduction Approach to the Synthesis of Copper Nanoparticles. *Int. Nano Lett.* **2016**, *6* (1), 21−26.
(35) Dankovich, T. A.; Smith, J. A. Incorporation of Copper Nanoparticles into Paper for Point-of-Use Water Purification. *Water Res.* **2014**, *63*, 245−251.
(36) Morsi, R. E.; Alsabagh, A. M.; Nasr, S. A.; Zaki, M. M. Multifunctional Nanocomposites of Chitosan, Silver Nanoparticles, Copper Nanoparticles and Carbon Nanotubes for Water Treatment: Antimicrobial Characteristics. *Int. J. Biol. Macromol.* **2017**, *97*, 264−269.
(37) Duan, L.; Zhao, Q.; Liu, J.; Zhang, Y. Antibacterial Behavior of Halloysite Nanotubes Decorated with Copper Nanoparticles in a Novel Mixed Matrix Membrane for Water Purification. *Environ. Sci.: Water Res. Technol.* **2015**, *1* (6), 874−881.
(38) Ramamoorthy, M.; Raju, M. D. Cellulose Acetate and Sulfonated Polysulfone Blend Ultrafiltration Membranes. Part III. Application Studies. *Ind. Eng. Chem. Res.* **2001**, *40* (22), 4815−4820.
(39) Rahimpour, A.; Madaeni, S. S. Polyethersulfone (PES)/Cellulose Acetate Phthalate (CAP) Blend Ultrafiltration Membranes: Preparation, Morphology, Performance and Antifouling Properties. *J. Membr. Sci.* **2007**, *305* (1−2), 299−312.
(40) Mbareck, C.; Nguyen, Q. T.; Alaoui, O. T.; Barillier, D. Elaboration, Characterization and Application of Polysulfone and Polyacrylic Acid Blends as Ultrafiltration Membranes for Removal of Some Heavy Metals from Water. *J. Hazard. Mater.* **2009**, *171* (1−3), 93−101.
(41) Chakrabarty, B.; Ghoshal, A. K.; Purkait, M. K. Preparation, Characterization and Performance Studies of Polysulfone Membranes Using PVP as an Additive. *J. Membr. Sci.* **2008**, *315* (1−2), 36−47.
(42) Shahlol, O. M. A.; Isawi, H.; El-Malky, M. G.; Al-Aassar, A. E.-H. M.; zwai, A. E. Performance Evaluation of the Different Nano-Enhanced Polysulfone Membranes via Membrane Distillation for Produced Water Desalination in Sert Basin-Libya. *Arabian J. Chem.* **2020**, *13* (4), 5118−5136.
(43) Ling, Z.; Wang, T.; Makarem, M.; Cintrón, M. S.; Cheng, H. N.; Kang, X.; Bacher, M.; Potthast, A.; Rosenau, T.; King, H.; Delhom, C. D.; Nam, S.; Edwards, J. V.; Kim, S. H.; Xu, F.; French, A. D. Effects of Ball Milling on the Structure of Cotton Cellulose. *Cellulose* **2019**, *26* (1), 305−328.
(44) French, A. D. Increment in Evolution of Cellulose Crystallinity Analysis. *Cellulose* **2020**, *27* (10), 5445−5448.
(45) Khalil, H. P. S. A.; Bhat, A. H.; Yusra, A. F. I. Green Composites from Sustainable Cellulose Nanofibrils: A Review. *Carbohydr. Polym.* **2012**, *87* (2), 963−979.
(46) Thomas, M. G.; Abraham, E.; Jyotishkumar, P.; Maria, H. J.; Pothen, L. A.; Thomas, S. Nanocelluloses from Jute Fibers and Their Nanocomposites with Natural Rubber: Preparation and Characterization. *Int. J. Biol. Macromol.* **2015**, *81*, 768−777.
(47) Shahinur, S.; Hasan, M.; Ahsan, Q.; Sultana, N.; Ahmed, Z.; Haider, J. Effect of Rot-, Fire-, and Water-Retardant Treatments on Jute Fiber and Their Associated Thermoplastic Composites: A Study by FTIR. *Polymers* **2021**, *13* (15), No. 2571.
(48) Badrinezhad, L.; Ghasemi, S.; Azizian-Kalandaragh, Y.; Nematollahzadeh, A. Preparation and Characterization of Polysulfone/Graphene Oxide Nanocomposite Membranes for the Separation of Methylene Blue from Water. *Polym. Bull.* **2018**, *75* (2), 469−484.
(49) Suh, I.-K.; Ohta, H.; Waseda, Y. High-Temperature Thermal Expansion of Six Metallic Elements Measured by Dilatation Method and X-Ray Diffraction. *J. Mater. Sci.* **1988**, *23* (2), 757−760.
(50) Mott, D.; Galkowski, J.; Wang, L.; Luo, J.; Zhong, C.-J. Synthesis of Size-Controlled and Shaped Copper Nanoparticles. *Langmuir* **2007**, *23* (10), 5740−5745.
(51) Zhou, R.; Wu, X.; Hao, X.; Zhou, F.; Li, H.; Rao, W. Influences of Surfactants on the Preparation of Copper Nanoparticles by Electron Beam Irradiation. *Nucl. Instrum. Methods Phys. Res., Sect. B* **2008**, *266* (4), 599−603.
(52) Martis, P.; Fonseca, A.; Mekhalif, Z.; Delhalle, J. Optimization of Cuprous Oxide Nanocrystals Deposition on Multiwalled Carbon Nanotubes. *J. Nanopart. Res.* **2010**, *12* (2), 439−448.
(53) Kooti, M.; Matouri, L. Fabrication of Nanosized Cuprous Oxide Using Fehling's Solution. *Sci. Iran.* **2010**, *17* (1), 73−78.
(54) Waseda, Y.; Matsubara, E.; Shinoda, K. *X-Ray Diffraction Crystallography: Introduction, Examples and Solved Problems*; Springer Science & Business Media, 2011.
(55) Sankar, R.; Maheswari, R.; Karthik, S.; Shivashangari, K. S.; Ravikumar, V. Anticancer Activity of Ficus Religiosa Engineered Copper Oxide Nanoparticles. *Mater. Sci. Eng.: C* **2014**, *44*, 234−239.
(56) French, A. D. Idealized Powder Diffraction Patterns for Cellulose Polymorphs. *Cellulose* **2014**, *21* (2), 885−896.
(57) Nishiyama, Y.; Sugiyama, J.; Chanzy, H.; Langan, P. Crystal Structure and Hydrogen Bonding System in Cellulose I $_{\alpha}$ from

https://doi.org/10.1021/acsomega.3c09966
ACS Omega 2024, 9, 34292−34302

Synchrotron X-Ray and Neutron Fiber Diffraction. *J. Am. Chem. Soc.* **2003**, *125* (47), 14300−14306.
(58) Wang, W.-m.; Cai, Z.; Yu, J.; Xia, Z. Changes in Composition, Structure, and Properties of Jute Fibers after Chemical Treatments. *Fibers Polym.* **2009**, *10* (6), 776−780.
(59) Cao, X.; Ding, B.; Yu, J.; Al-Deyab, S. S. Cellulose Nanowhiskers Extracted from TEMPO-Oxidized Jute Fibers. *Carbohydr. Polym.* **2012**, *90* (2), 1075−1080.
(60) Cai, M.; Takagi, H.; Nakagaito, A. N.; Katoh, M.; Ueki, T.; Waterhouse, G. I. N.; Li, Y. Influence of Alkali Treatment on Internal Microstructure and Tensile Properties of Abaca Fibers. *Ind. Crops Prod.* **2015**, *65*, 27−35.
(61) Nasirian, D.; Salahshoori, I.; Sadeghi, M.; Rashidi, N.; Hassanzadeganroudsari, M. Investigation of the Gas Permeability Properties from Polysulfone/Polyethylene Glycol Composite Membrane. *Polym. Bull.* **2020**, *77* (10), 5529−5552.
(62) Lin, L.; Qiu, P.; Cao, X.; Jin, L. Colloidal Silver Nanoparticles Modified Electrode and Its Application to the Electroanalysis of Cytochrome c. *Electrochim. Acta* **2008**, *53* (16), 5368−5372.
(63) Sankar, R.; Karthik, A.; Prabu, A.; Karthik, S.; Shivashangari, K. S.; Ravikumar, V. Origanum Vulgare Mediated Biosynthesis of Silver Nanoparticles for Its Antibacterial and Anticancer Activity. *Colloids Surf., B* **2013**, *108*, 80−84.
(64) César, N. R.; Pereira-da-Silva, M. A.; Botaro, V. R.; de Menezes, A. J. Cellulose Nanocrystals from Natural Fiber of the Macrophyte Typha Domingensis: Extraction and Characterization. *Cellulose* **2015**, *22* (1), 449−460.
(65) Arifuzzaman Khan, G. M.; Shaheruzzaman, M.; Rahman, M. H.; Abdur Razzaque, S. M.; Islam, M. S.; Alam, M. S. Surface Modification of Okra Bast Fiber and Its Physico-Chemical Characteristics. *Fibers Polym.* **2009**, *10* (1), 65−70.
(66) Yan, Y.; Zhang, M.; Gong, K.; Su, L.; Guo, Z.; Mao, L. Adsorption of Methylene Blue Dye onto Carbon Nanotubes: A Route to an Electrochemically Functional Nanostructure and Its Layer-by-Layer Assembled Nanocomposite. *Chem. Mater.* **2005**, *17* (13), 3457−3463.
(67) Roy, A.; Chakraborty, S.; Kundu, S. P.; Adhikari, B.; Majumder, S. B. Adsorption of Anionic-Azo Dye from Aqueous Solution by Lignocellulose-Biomass Jute Fiber: Equilibrium, Kinetics, and Thermodynamics Study. *Ind. Eng. Chem. Res.* **2012**, *51* (37), 12095−12106.
(68) Manna, S.; Roy, D.; Saha, P.; Gopakumar, D.; Thomas, S. Rapid Methylene Blue Adsorption Using Modified Lignocellulosic Materials. *Process Saf. Environ. Prot.* **2017**, *107*, 346−356.
(69) Rinna, F.; Buono, S.; Cabanelas, I. T. D.; Nascimento, I. A.; Sansone, G.; Barone, C. M. A. Wastewater Treatment by Microalgae Can Generate High Quality Biodiesel Feedstock. *J. Water Process Eng.* **2017**, *18*, 144−149.
(70) Satapathy, M. K.; Das, P. Optimization of Crystal Violet Dye Removal Using Novel Soil-Silver Nanocomposite as Nanoadsorbent Using Response Surface Methodology. *J. Environ. Chem. Eng.* **2014**, *2* (1), 708−714.

https://doi.org/10.1021/acsomega.3c09966
ACS Omega 2024, 9, 34292−34302